

Influence of Sr²⁺ substitution on structural, optical and catalytic properties of CoAl₂O₄ nanoparticles

G. Anitha^{a*}, R. Jothiramalingam^b, M. Sukumar^c, A. Roniboss^d, S. Yuvaraj^e,
G. Ramkumar^a, M. Sundararajan^f, S. Arokiyaraj^g

^a*Department of Electronics and Communication Engineering, Saveetha School of Engineering, Saveetha Institute of Medical and Technical Sciences, Saveetha University, Chennai, 602105, Tamil Nadu, India*

^b*Chemistry Department, College of Science, King Saud University, P.O. Box. 2455, Riyadh 11451, Saudi Arabia*

^c*Department of Applied Physics, Sri Venkateswara College of Engineering, Pennallur, Sriperumbudur, Tamil Nadu, 602 117, India*

^d*Department of Chemistry, Vel Tech Rangarajan Dr.Sagunthala R&D Institute of Science and Technology, Chennai-600062, Tamilnadu, India*

^e*Department of Physics, Vel Tech Rangarajan Dr.Sagunthala R&D Institute of Science and Technology, Chennai-600 062, Tamilnadu, India*

^f*PG& Research Department of Physics, Paavendhar College of Arts & Science, M.V. South, Attur, Salem 636 121, Tamilnadu, India*

^g*Department of Food Science and Biotechnology, Sejong University, South Korea*

Strontium substituted CoAl₂O₄ nanoparticles were prepared using a microwave combustion technique using L-alanine as a fuel. The following techniques were used to test the synthesized samples such as XRD, HR-SEM, EDX, DRS, FT-IR and VSM respectively. Surface morphology showed nanosized crystalline grains agglomerated with flake-like and nano-sized pores are fused grain boundaries. The band gap was calculated using Kubelka-Munk (K-M) function and it is reduced from 3.32 to 3.18 eV. The FT-IR bands ranging from 560 to 1100 cm⁻¹ are caused by the cubic structure of Sr²⁺ doped CoAl₂O₄ nanoparticles (NPs). The bi-functional NPs CoAl₂O₄/SrO (x = 0.5) exhibited excellent catalytic performance and better conversion efficiency (conversion 98% and selectivity 95%) for glycerol.

(Received May 1, 2023; Accepted July 31, 2023)

Keywords: Cubic spinel, CoAl₂O₄ NPs, Optical properties, Super paramagnetic-materials, Glycerol oxidation

1. Introduction

In recent years, semiconductor materials have great deal of attention in the fields of nano-science and nanotechnology due to their exceptional optical, electrical, thermal, and magnetic properties. Metal oxides have recently used in photocatalytic degradation [1], optical sensors [2], energy storage, resistive memory chips [3,4] and super capacitors [5] and so on. Cobalt aluminate is thought to be a good choice for sensor applications because of its diffusion is good, surface acidity is low, thermal resistance is increased, improved mechanical resistance, thermal stability, and hydrophobicity is enhanced [6]. Because of these materials has mechanical [7], electric [8, 9] and optical properties, [10] it makes suitable to use as energy carriers, catalytic [11], nano-pigments [12] and hyperthermia application [13]. The divalent metal ion (Co²⁺) is represented by the tetrahedral A-site, whereas the trivalent metal ion (Al³⁺) is represented by the octahedral B-site [6]. The cobalt aluminate structure was selected because of its, excellent structural, optical, morphological and magnetic properties.

* Corresponding author: anipsg09@gmail.com
<https://doi.org/10.15251/DJNB.2023.183.915>

Throughout the reported work, all aluminates of spinel metals, nanomaterial of cobalt aluminate is well known semiconducting material with a wide band gap values (3.5 to 3.9 eV) [14, 15]. CoAl_2O_4 , an exceptional inorganic with a regular spinel structure, has outstanding, magnetic, electrical, and optical properties [16, 17]. As a catalyst, cobalt aluminate is used for various reaction at high-temperature [18,19] and also in optical property applications [20, 21]. Due to high magnetic activity of cobalt aluminate with cubic spinel form in order to promising candidate for photo-catalysts [8]. The “magnetic (M), optical (O), electrical (E), and structural (S) properties” for their host material, and also for the chemical structure of the host material, can all be improved by doping strontium ions into the matrix. The addition of strontium ions is changing the host material's entire structure (from standard spinel to reverse spinel) and improves its magnetic properties. [21, 22]. Strontium doped metal aluminates, in particular, used in various applications such as gas sensor device, large storing device and spintronic device [22]. The percentage of Sr^{2+} ions in zinc aluminate affects the magnetic properties of Co-Sr spinel aluminates in particular. Co-Sr aluminates have a higher resistivity, initial permeability, and magnetic saturation, making them a better candidate for inductors, electrical MEMS switches, and microwave systems [23], converters, aerial cores [24,25] and devices in memory applications [26, 27]. Cobalt aluminates spinel can be made in a variety of forms, including solid-state reaction [28], hydrothermal [29], microwave combustion [30, 31] and reverse miscelle surfactant applications [32]. The high efficiency, ultra-fine and unalloyed fine particles using microwave combustion technique is a simple and appealing process for synthesizing cobalt aluminate at nanoscale. Propylene glycol, urea and citric acid are commonly used for fuels in the combustion technique to synthesis cobalt aluminates [33]. Despite many available cobalt aluminates nanoparticles, the combination of cobalt aluminates (metal precursors) with L-alanine used as a fuel is not reported in the past.

Toni et al., 2020 described the microwave combustion method to synthesize $\text{Cu}_{1-x}\text{Zn}_x\text{Fe}_2\text{O}_4$ NPs. The crystalline nature and lattice constants are calculated to be 15 to 19 nm and 8.319 to 8.400 Å respectively [34]. The electrical conductivity was determined using the Kubelka-Munk formula and was determined to be between 2.30 and 2.51eV [35]. *Lahde et al.*, 2017 proposed a paper related to a nano-particles premised on cobalt aluminium spinel produced by flaming thermal oxidation for different catalysts [33], the authors have also explained the catalysis characteristics of CoAl spinel nano-particles. L-alanine is used as a fuel for the combustion process to prepare Sr^{2+} doped CoAl_2O_4 NPs. Hence, in the present study demonstrates the effects of Sr^{2+} doping on structural, optical, and catalytic activity of CaAl_2O_4 by X-ray diffraction (XRD), scanning electron microscopy (SEM) and energy dispersive X-ray analysis (EDX), diffuse reflectance spectroscopy (DRS), Fourier transform infrared spectroscopy (FTIR) techniques. To investigate the catalytic property of as prepared nanoparticles have studied using catalytic oxidation of glycerol as a test reaction.

2. Experimental

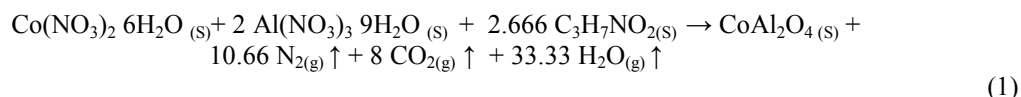
2.1. Materials

Cobalt nitrate ($\text{Co}(\text{NO}_3)_2 \cdot 6\text{H}_2\text{O}$), aluminium nitrate ($\text{Al}(\text{NO}_3)_3 \cdot 9\text{H}_2\text{O}$), strontium nitrate ($\text{Sr}(\text{NO}_3)_2 \cdot 9\text{H}_2\text{O}$) and L-alanine ($\text{C}_3\text{H}_7\text{NO}_2$) were analytical grade (99.9%), purchased from SD fine-chemicals, India. All these chemicals were used as received without further purification. Double distilled water was used during sample preparation.

2.2. Synthesis of $\text{Co}_{1-x}\text{Sr}_x\text{Al}_2\text{O}_4$ nanoparticles

Metal nitrates (Cobalt/Strontium – 1 mole and Aluminum – 2 moles) were used as precursors in addition to L-alanine as fuel for the synthesis of nanoparticles by combustion technique. The propellant chemistry concept of fuel to oxidizer (F/O) was supposed to equal 1. An homogeneous solution was obtain by dissolving the constituents in the desired mole ratio (1:2 mole ratio) in de-ionized water followed by stirring at room temperature for 30 min and it was poured into a cylindrically shaped pure silica crucible and placed at the center of oven for irradiation procedure, which is initially set to 120 min at 100 °C. The solution boiled while delivering heat energy, vaporizing, dehydrating, and decomposing with reaction gas evolution. As

the solution entered natural combustion, ignition occurred, resulting in the rapid development of $\text{Co}_{1-x}\text{Sr}_x\text{Al}_2\text{O}_4$ ($0 \leq x \leq 0.5$) NPs in a flame fluffy fashion. Finally, the obtained sample was cleaned with distilled water and ethanol before being dried for two hours at 500 °C (using muffle furnace). COA1, COSA2, COSA3, and COSA4 are the names of the final products. The chemical reactions involved in the formation of $\text{Co}_{1-x}\text{Sr}_x\text{Al}_2\text{O}_4$ ($0 \leq x \leq 0.5$) NPs are as follows:



2.3. Characterizations

The crystalline structure and phase of as-prepared cobalt aluminate NPs are characterized using radiation of $\text{CuK}\alpha$ at $\lambda = 1.5406$ in the range of 20° to 80° in the radiation of 20 (Model Rigaku Ultima III). An X-ray analyzer for energy dispersive is fitted with an EIKO IB2 scanning electron microscope for morphology and elemental analysis characterization. The diffuse reflectance spectrums have been obtained using a Perkin Elmer twin beam spectro-photometer in the wavelength ranges 200-800 nm (Thermo Scientific Evolution 220). The FT-IR spectrums were collected using a spectro-photometer from Thermo Scientific (LYZA 500).

2.4. Catalytic activity

The conversion of glycerol was carried out in a batch reactor operating under atmospheric conditions using a two-necked round bottom (250 ml) flask equipped with reflux condenser and temperature controller. 0.05 mole of oxidant (hydrogen peroxide) was added along with a 50 mg of the catalyst then heated at 80 °C in acetonitrile medium for 6 h. The liquid phase products were analyzed by Agilent 1100 gas chromatography (GC) equipped with an Abel Bonded (AB-1, Capillary) column (30 m × 0.25 mm × 0.25 μm) and FID detector. Products were identified by using Agilent Technologies Model 7890A gas chromatography mass spectrometer (GC-MS) coupled to a mass detector model 5975 C and HP-5MS (30 m × 250 μm × 0.25 μm) column.

3. Results and discussion

3.1. X-rays diffraction analysis

Fig. 1 displays the pattern of X-ray diffraction for prepared strontium doped cobalt aluminate NPs. It is observed that the entire diffraction pattern indicates the good crystalline structure. The 2θ values of 31.21, 36.75, 44.79, 55.53, 59.28, and 65.18 correlate to the reflection planes of Sr doped cobalt aluminate (220), (311), (400), (422), (511), and (440). The distribution information (JCPDS card number 82-2239) exhibiting the cubic spinel arrangement with the space collection Fd-3m [24] corresponds exactly to all of the dispersed peaks [24]. The SrO NPs exhibit deteriorated peaks at 2θ values of 26.51, which is consistent with the Sr doped CoAl_2O_4 system. Using the (311) reflection plane, Debye Scherrer's Eq. (2) was utilized to determine the average crystallite size (L) and all calculated XRD parameters are given in Table 1.

$$L = \frac{0.89\lambda}{\beta \cos \theta} \quad (2)$$

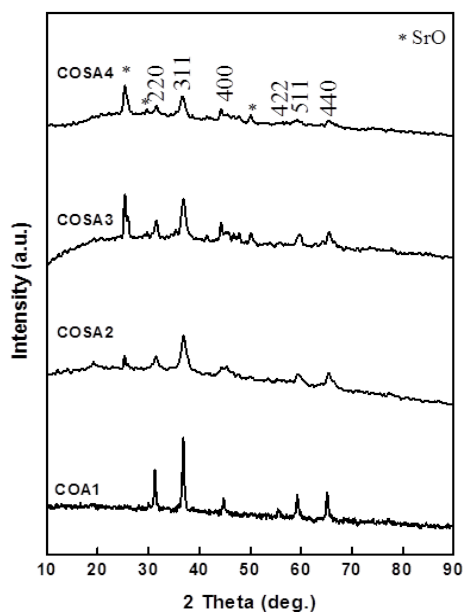


Fig. 1. XRD spectra of Sr^{2+} doped CoAl_2O_4 NPs.

Table 1. Crystallite size, lattice parameter and energy gap of $\text{Co}_{1-x}\text{Sr}_x\text{Al}_2\text{O}_4$ ($0 \leq x \leq 0.5$) spinel NPs.

Sample code	Sample Name	Crystallite Size, L (nm)	Lattice Parameter, a (Å)	Energy gap (eV)
COA1	CoAl_2O_4	14.40	8.111	3.32
COSA2	$\text{Co}_{0.9}\text{Sr}_{0.1}\text{Al}_2\text{O}_4$	16.10	8.114	3.28
COSA3	$\text{Co}_{0.7}\text{Sr}_{0.3}\text{Al}_2\text{O}_4$	18.15	8.119	3.20
COSA4	$\text{Co}_{0.5}\text{Sr}_{0.5}\text{Al}_2\text{O}_4$	20.01	8.122	3.18

L , is the average crystalline size; β , is the full width at half maximum (FWHM) of the detected diversion peak; and θ , is the diffraction angle. The diffraction peak (311) of strontium doped cobalt aluminate has an average crystallite dimension of 14 to 20 nm. Eq. 3 was used to measure the lattice parameter for the $\text{Co}_{1-x}\text{Sr}_x\text{Al}_2\text{O}_4$ ($0 \leq x \leq 0.5$) NPs.

$$a = d_{hkl} \sqrt{(h^2 + k^2 + l^2)} \quad (3)$$

where, d_{hkl} , is the the miller indices are given by the equivalent interatomic spacing;

The crystal planes denote h , k , l and a -denotes the lattice parameter. The cubic spinel structure is described by the lattice parameter ' a ', which ranges from 8.111 to 8.122 Å. The determined lattice parameter ' a ' agrees well with the previously published value of 8.106 Å.

3.2. SEM and EDX analysis

The surface morphology of Sr^{2+} doped CoAl_2O_4 NPs is studied using HR-SEM technique. The images observed cobalt aluminate NPs which notable tendency of coalescence agglomerated, aggregation, nano-sized porous with fused grain boundary morphology are shown in Fig. 2. Because of the lower energy release during the combustion process, spherical morphology and agglomerated has the $\text{Co}_{1-x}\text{Sr}_x\text{Al}_2\text{O}_4$ ($0 \leq x \leq 0.5$) NPs. Fig. 3 depicts the elemental composition of $\text{Co}_{1-x}\text{Sr}_x\text{Al}_2\text{O}_4$ ($0 \leq x \leq 0.5$) NPs as evaluated by energy dispersive X-ray analysis. The peaks

correspond to Co, Sr, Al, and O, indicating that the cobalt aluminate and strontium doped cobalt aluminate NPs are highly substituted.

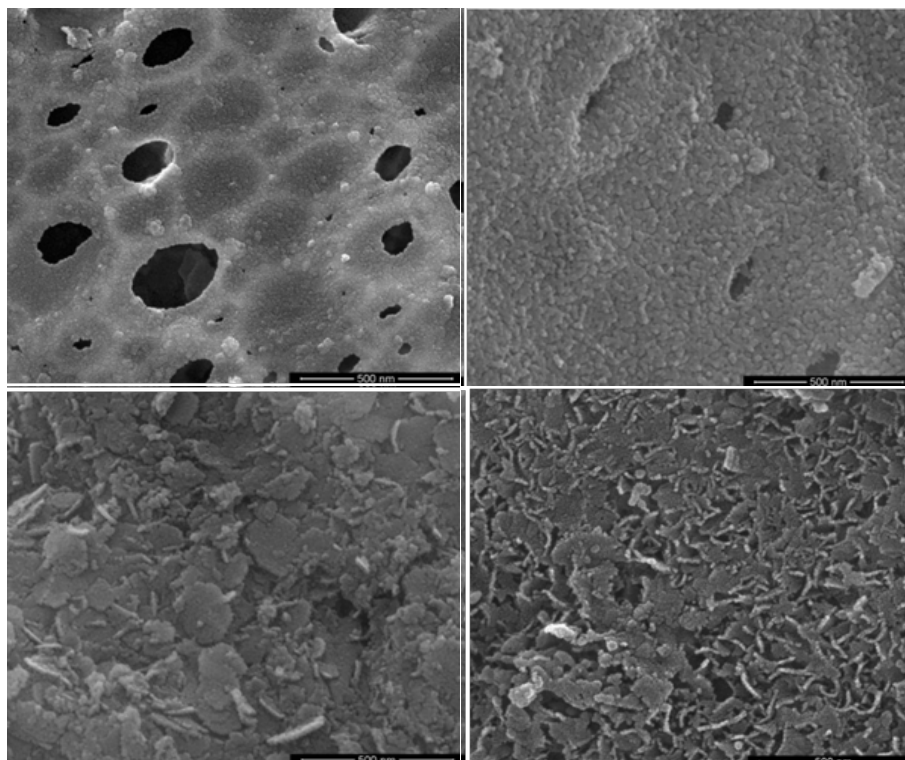


Fig. 2. HR-SEM analysis of Sr^{2+} doped $CoAl_2O_4$ NPs.

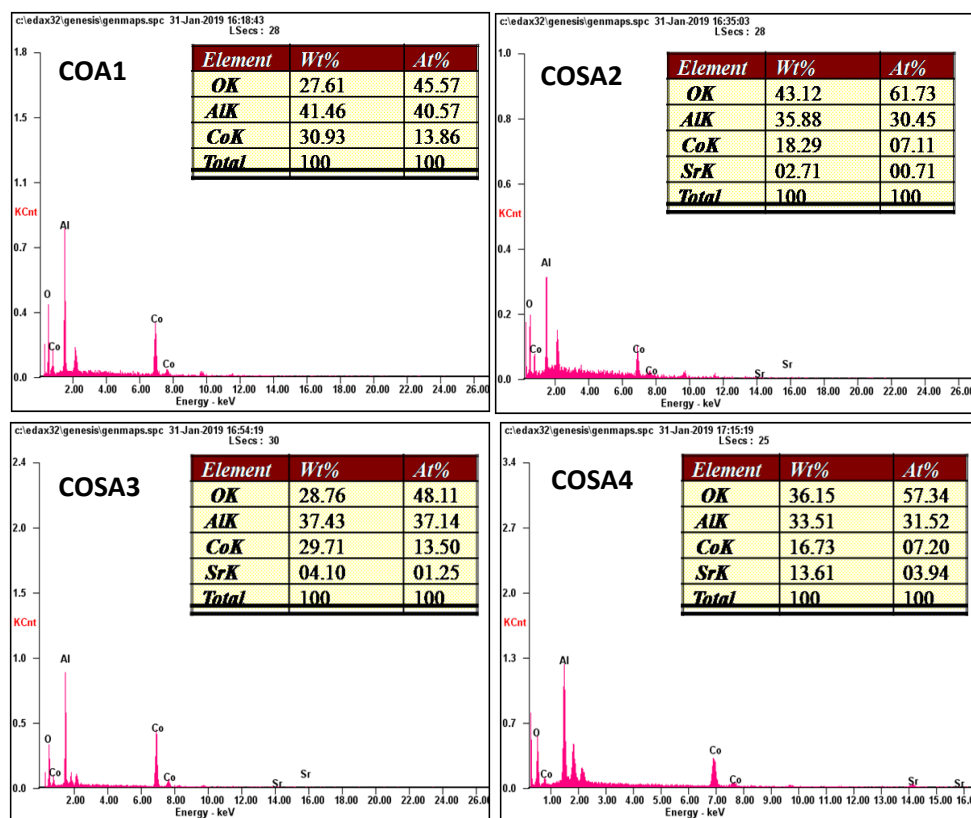


Fig. 3 EDX spectra of Sr^{2+} doped $CoAl_2O_4$ NPs.

3.3. Optical properties

The energy band gap of Sr²⁺ doped CoAl₂O₄ NPs is persistent using spectroscopy of diffuse reflectance in the ultraviolet visible region [33, 34]. The Tauc connection is a mathematical proof that is used to determine the energy difference and as specified in the equation. The diffused reflectance was converted to an absorption coefficient using the Kubelka-Munk function $F(R)$ (4).

$$\alpha = F(R) = \frac{(1-R)^2}{2R} \quad (4)$$

$F(R)$, is the Kubelka-Munk function and R , is the reflectance. The equation expresses the Tauc relationship (5),

$$F(R)hv = A(hv - E_g)^n \quad (5)$$

Hence, $n = 2$ and $\frac{1}{2}$, which is imply the permissibility of indirect and direct transitions, respectively. In Fig. 4, a Tauc plot is shown among $(F(R)hv)^2$ and band gap (hv), with linear points in the strategies extrapolated to $(F(R)hv)^2 = 0$, yielding the expected straight band gap. The direct band gaps of strontium doped cobalt aluminate NPs were 3.56 eV, 3.47 eV, 3.42 eV, and 3.35 eV, respectively. The reduction in optical band gap standards as increases the strontium dopant concentration is due to the addition of new energy levels in between the energy bands [33].

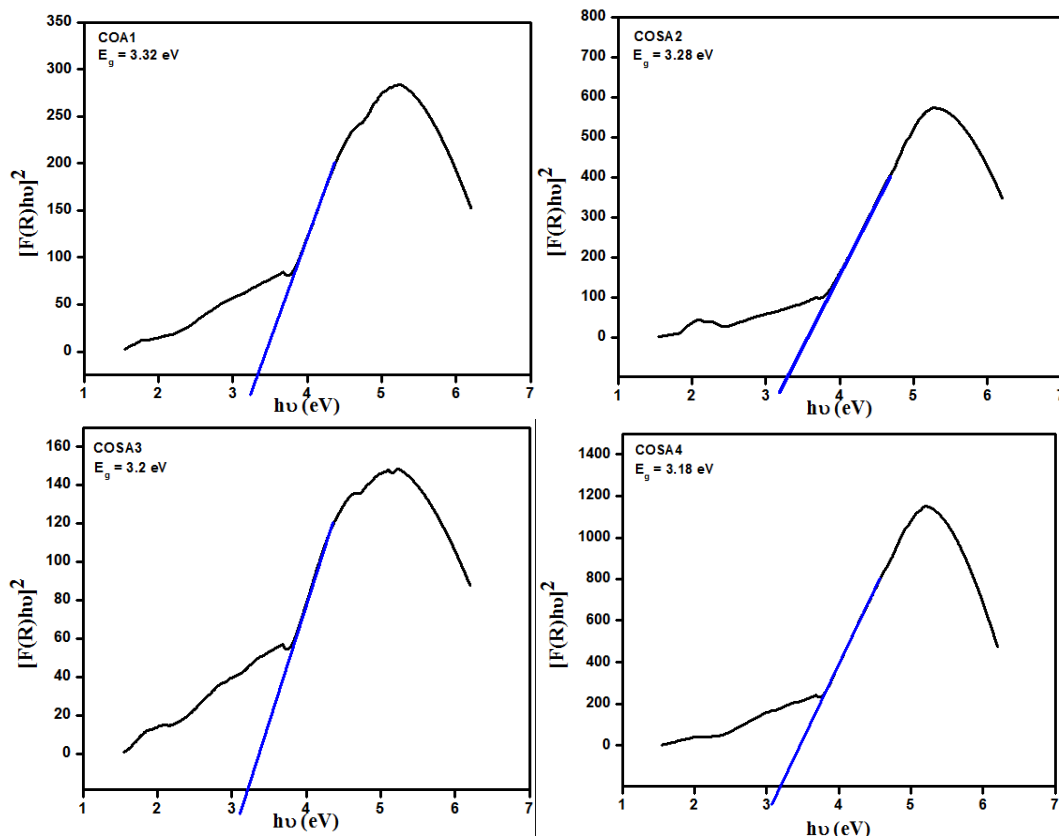


Fig. 4. $(F(R)hv)^2$ vs band gap of $Co_{1-x}Sr_xAl_2O_4$ ($0 \leq x \leq 0.5$) NPs.

3.4. FT-IR analysis

The FT-IR spectrum of $Co_{1-x}Sr_xAl_2O_4$ ($0 \leq x \leq 0.5$) NPs formed by burning is shown in Fig. 5. At room temperature, the FT-IR spectrum was obtained in the range 4000-400 cm^{-1} . The wide band at 3439 cm^{-1} is reserved for water molecule absorption via -OH stretching vibrations. The band between 2920 and 2847 cm^{-1} [36] regulates the C-H enlarging vibration of hydrogen-

bonded molecules. The absorption bands at 1631 and 1435 cm^{-1} on the particle surface are induced by the presence of organic molecules and their coordination with amino and carboxyl groups (e.g. COO^-). The bands between 560 and 1100 cm^{-1} are caused by the cubic structure of CoAl_2O_4 NPs doped with Sr^{2+} [37].

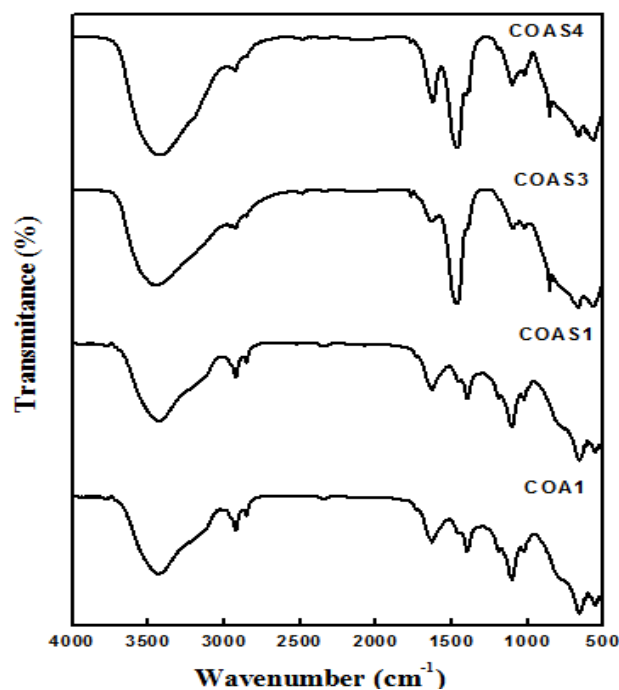


Fig. 5 FT-IR spectra of Sr^{2+} doped CoAl_2O_4 NPs.

3.6. Catalytic activities

3.6.1. Effect sample composition

The $\text{Co}_{1-x}\text{Sr}_x\text{Al}_2\text{O}_4$ ($0 \leq x \leq 0.5$) spinel catalyst for oxidation of glycerol was carried out under atmospheric conditions was carried out using 50 mg catalyst at 80 °C for 6 h and final results are shown in Fig. 6.

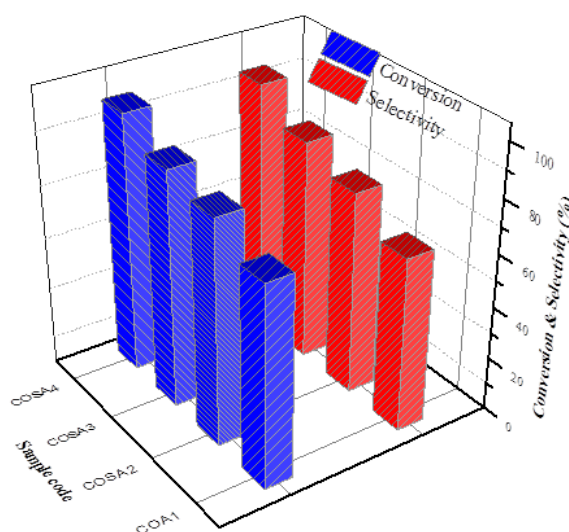


Fig. 6 Effect of Sr^{2+} doping fraction.

The results shows increased conversion and selectivity for glycerol oxidation. The strontium concentration ranges from $x = 0.0$ to 0.5, it is linearly increases the conversion from 75.6% to 98.2% and selectivity was 65.7% to 94.8% respectively. Among, all the catalyst samples, the COSA4 is a most promising and it achieved good conversion towards glycerol. Hence, the importance of strontium doped cobalt oxide with spinel structure was achieved.

3.6.2. Influence of the catalyst weight of the COSA4 nanoparticle

The glycerol conversion (52.4 to 99%) and selectivity (49.5% to 94.8%) get linearly increased, on growing the catalytic stuffing from 20 to 70 mg and it is shown in Fig. 7. The discrimination of formic acid reductions to 90.5% leading to pore blocking and reactive surface decline on using the catalyst over 70 mg [38]. The ideal catalyst amount to attain high catalyst activity is 50 mg, which is been discovered from the results.

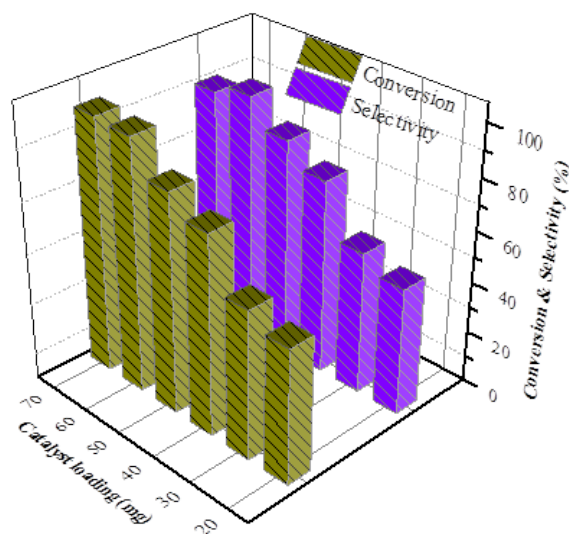


Fig. 7 Effect of catalyst loading.

3.6.3. Recycling performance of COSA4 catalyst

From the investigation of the reusability (Fig. 8) of COSA4 catalyst during glycerol conversion indicates that the catalyst was improved through purifying and washing with purified water numerous times followed by drying at 180 °C for 2.5 h in warm air oven.

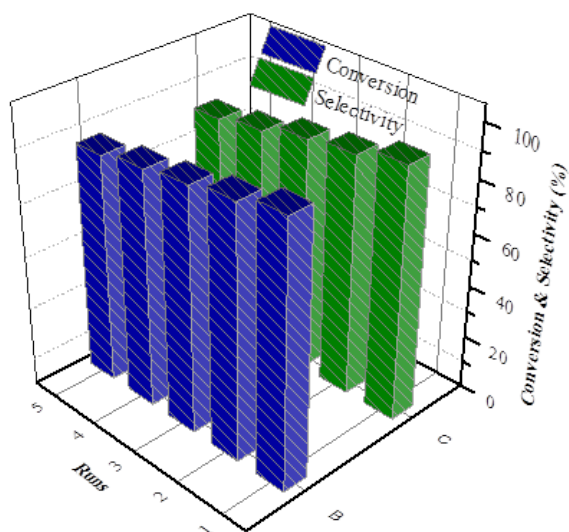
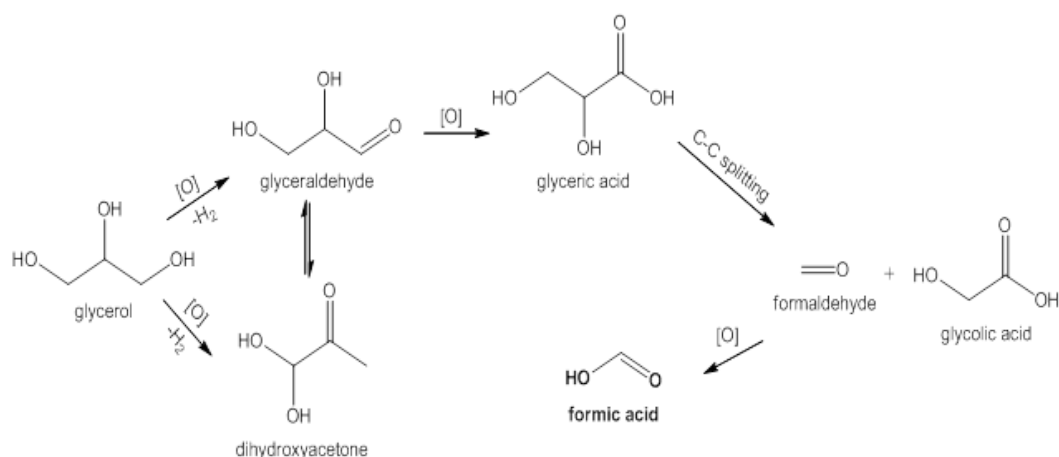


Fig. 8 Reusability studies on the COSA4 catalyst.

Under identical condition the reprocessed catalyst is utilized for about afterward four turns. The oxidation of glycerol (from 98.2 to 82%) and the exercising judgment of formic acid (94.8 to 75%) slightly decrease. This decrease is probably due to bulk loss of the chemical agent during laundry and retrieval process [40].

3.6.4. Reaction pathway

Scheme 1 shows the reaction process for converting glycerol to formic acid from an experiment carried out with a COSA4 spinel catalyst in an acetonitrile medium. The glycerol is first oxidized to either glyceraldehyde or dihydroxyacetone. On further oxidation, glyceraldehyde is transformed into glyceric and tartronic acid, and the glyceric acid undergoes rapid C–C bond breakage to create glycolic acid and formaldehyde, which in turn forms formic acid on further oxidation. Meanwhile, dihydroxyacetone may generate glyceraldehyde under keto-enol tautomerism and, with further oxidation, glycolic acid, and, as previously mentioned, formaldehyde and formic acid.



Scheme 1. Possible reaction pathway for catalytic oxidation of glycerol using COSA4 spinel catalyst.

4. Conclusion

The combustion approach was utilized to synthesize $\text{Co}_{1-x}\text{Sr}_x\text{Al}_2\text{O}_4$ ($0 \leq x \leq 0.5$) NPs using L-alanine as a fuel. Undoped CoAl_2O_4 (COA1) and Sr^{2+} doped CoAl_2O_4 (COSA2 and COSA3) showed a single phase with cubic structure. Further doping (COSA4) led to form a bi-functional phase of $\text{CoAl}_2\text{O}_4/\text{SrO}$ nanoparticles. However, increase doping concentration, the value lattice parameter improved from 8.112 Å to 8.122 Å. HR-SEM revealed the crystalline materials with nano-porous and flake like images. EDX observation confirmed the existence of Co, Sr, Al, and O elements. The band gap value of 3.32 eV to 3.18 eV was deduced by $\text{Co}_{1-x}\text{Sr}_x\text{Al}_2\text{O}_4$ ($0 \leq x \leq 0.5$) spinel NPs. FT-IR spectra showed the vibrational stretching modes corresponding to the CoAl_2O_4 spinel structure. Sr^{2+} doped CoAl_2O_4 NPs show high performance in catalyzing glycerol oxidation. Among the different compositions, COSA4 exhibits the maximum catalytic activity for the oxidation of glycerol to formic acid (98.2%). A reaction mechanism is proposed.

Acknowledgements

The authors (Jothi Ramalingam Rajabathar) acknowledge the financial support through Researchers Supporting Project number (RSP2023R354) King Saud University, Riyadh 11451, Saudi Arabia.

References

- [1] M. Sundararajan, L.J. Kennedy, *J. Environ. Chem. Engineer.*, 5 (2017) 4075-4092; <https://doi.org/10.1016/j.jece.2017.07.054>
- [2] M. Maruthupandy, Y. Zuo, J.S. Chen, J.M. Song, H.L. Niu, C.J. Mao, S.Y. Zhang, Y.H. Shen, *Appl. Sur. Sci.* 397 (2017) 167-174; <https://doi.org/10.1016/j.apsusc.2016.11.118>
- [3] B. Beheraa, S. Maity, K. Ajit, S. Das, *Superlatt. Microstruct.* 117 (2018) 298-304; <https://doi.org/10.1016/j.spmi.2018.03.036>
- [4] M Agila, S Krithiga, *Int. j. eng. sci. manag. res.* 2(2), 2581 (2019).
- [5] K. Prasanna, P. Santhoshkumar, Y.N. Joa, I.N. Sivagami, S.H. Kanga, Y.C. Joe, C.W. Lee, *Appl. Sur. Sci.* 449 (2018) 454 – 460; <https://doi.org/10.1016/j.apsusc.2017.12.130>
- [6] C. Wang, S. Liu, L. Liu, X. Bai, *Mater. Chem. Phys.* 96 (2) (2006) 361-370; <https://doi.org/10.1016/j.matchemphys.2005.07.066>
- [7] S. Zhao, J. Guo, W. Li, H. Guo, B. You, *Dyes and Pigment.* 151 (2018) 130-139; <https://doi.org/10.1016/j.dyepig.2017.12.062>
- [8] Xuanmeng He, Wenjie Zhu, Xinzhen Wang, Fen Wang, Hui Liu & Zehua Lei, *J. Mater. Sci.*, 55, (2020) 3569-13577; <https://doi.org/10.1007/s10853-020-04967-y>
- [9] Chandra Sekhar Dash, Jothi ramalingam Rajabathar, Hamad Al-Lohedan, Selvaraj Arokiyaraj, S. Ramachandran, M. Sukumar, R. Revathi, G. Anitha & M. Sundararajan (2022) *Inorg. Nano-Met. Chem.*
- [10] D. Dhak, P. Pramanik, *J. Am. Ceram. Soc.* 89 (2006)1014-1021; <https://doi.org/10.1111/j.1551-2916.2005.00769.x>
- [11] N. Ouahdi, S. Guillemet, J.J. Demai, B. Durand, L. ErRakho, R. Moussa, A. Samdi, *Mater. Lett.* 59 (2005) 334-340; <https://doi.org/10.1016/j.matlet.2004.10.013>
- [12] T. Tatarchuk, N. Danyliuk V. Kotsyubynsky, A. Shumskaya, A.A. Ghfar, Mu. Naushad, A. Shyichuk, *Chemosphere* 294 (2022) 133565; <https://doi.org/10.1016/j.chemosphere.2022.133565>
- [13] T. Tatarchuk, A. Shyichuk, J. Lamkiewicz, J. Kowalik, *Ceramics International*, 46 (10) 2(020) 14674-14685; <https://doi.org/10.1016/j.ceramint.2020.02.269>
- [14] T. Tatarchuk, A. Shyichuk, Z. Sojka, J. Gryboś, M. Naushad, V. Kotsyubynsky, M. Kowalska, S. K. Marks, N. Danyliuk, *Journal of Molecular Liquids*, 328 (2021) 115375; <https://doi.org/10.1016/j.molliq.2021.115375>
- [15] C.S. Dash, J.R. Rajabathar, H.L. Lohedan, S. Arokiyaraj, S. Ramachandran, *Inorg. Nano-Met. Chem.*
- [16] M. Sales, C. Valentín, J. Ala, *J. Eur. Ceram. Soc.* 17 (1997) 41-47; [https://doi.org/10.1016/S0955-2219\(96\)00069-6](https://doi.org/10.1016/S0955-2219(96)00069-6)
- [17] Zhang, X., Shi, F., Yu, X., Liu, H., Fu, Y., Wang, Z.Q., Jiang, L., Li, X.Y., *J. Am. Chem. Soc.* 126, 3064-3065; <https://doi.org/10.1021/ja0398722>
- [18] S.H. Jazayeri, F. Bondioli, A. Allahverdi, M. Shirvani, A.M. Ferrari, *Int. J. Appl. Ceram. Technol.* 9 (2012) 968-978; <https://doi.org/10.1111/j.1744-7402.2011.02704.x>
- [19] A.S. Gorgani, E. Bakhshandeh, F. Najafi, *J. Eur. Ceram. Soc.* 34 (2014) 2959-2967; <https://doi.org/10.1016/j.jeurceramsoc.2014.04.030>
- [20] A.T. Raghavender, K. Zadro, D. Pajic, Z. Skoko, N. Billiskov, *Mater. Lett.* 64 (2010) 1144-1146; <https://doi.org/10.1016/j.matlet.2010.02.031>
- [21] M. Sundararajan, L.J. Kennedy, *J. Environ. Chem. Engineer.*, 5 (2017) 4075-4092; <https://doi.org/10.1016/j.jece.2017.07.054>
- [22] M.A.F. Ramalho, L. Gama, S.G. Antonio, C.O. Paiva-Santos, E.J. Miola, R.H.G.A. Kiminami, A.C.F.M. Costa, *J. Mater. Sci.* 42 (2007) 3603-3606; <https://doi.org/10.1007/s10853-006-0383-2>
- [23] Y.K. Sun, I.H. Oh, S.A. Hong, *J. Mater. Sci.* 31 (1996) 3617-3621; <https://doi.org/10.1007/BF00352769>
- [24] Gopalan, A., & Kommuri, U. K, *J. Appl. Surface Sci.*, 449 (2018) 340-345;

<https://doi.org/10.1016/j.apsusc.2018.02.210>

[25] M. Sukumar, LJ Kennedy, JJ Vijaya, B Al-Najar, M Bououdina, G Mudhana, Vacuum, 167 (2019) 407-415; <https://doi.org/10.1016/j.vacuum.2019.06.036>

[26] A. Alarifi, N.M. Deraz, S. Shaban, J. Alloys Compd. 486 (2009) 501-506;
<https://doi.org/10.1016/j.jallcom.2009.06.192>

[27] A. Roniboss, S. Subramani, R. Ramamoorthy, S. Yuvaraj, M. Sundararajan, and Chandra Sekhar Dash, Mater. Sci. in Semicond. Proces. (2020): 105507;
<https://doi.org/10.1016/j.mssp.2020.105507>

[28] D. Gingașu, I. Mindru, L. Patron, G. Marinescu, A. Ianculescu, Y.A. Surdu, S. Somacescu, S. Preda, O. Oprea, Rev. Roum. Chim. 63 (5-6) (2018) 459-466.

[29] Alexandre A. S. Goncalves, Maria J. F. Costa, Liping Zhang, Filip Ciesielczyk, and Mietek Jaroniec, Chemistry of Materials 30 (2), (2018) 436-446.

[30] Zhi-Zhan Chen, Er-Wei Shi, Wen-Jun Li, Yan-Qing Zheng, Ji-Yong Zhuang, Bing Xiao, Lian-An Tang, Materials Science and Engineering: B, 107 (2) (2004) 217-223;
<https://doi.org/10.1016/j.mseb.2003.11.013>

[31] Sofia, N. Iyandurai, S. Yuvaraj, and M. Sundararajan, Materials Research Express 7, no. 4 (2020): 046104; <https://doi.org/10.1088/2053-1591/ab7a7a>

[32] G.T. Anand, L.J. Kennedy, J.J. Vijaya, K. Kaviyaran, M. Sukumar, Ceram. Int. 41 (2014) 603-615; <https://doi.org/10.1016/j.ceramint.2014.08.109>

[33] J. Chandradass, M. Balasubramanian, K.H. Kim, J. Alloys Compd. 506 (2010) 395-399;
<https://doi.org/10.1016/j.jallcom.2010.07.014>

[34] A. Lahde, R.J. Chimentão, T. Karhunen, M.G. Álvarez, J. Llorca, F. Medina, J. Jokiniemi, L.B.M. Lopez, Advanced Powder Technology, 28 (2017) 3296-3306;
<https://doi.org/10.1016/j.apt.2017.10.009>

[35] M. Zayat, D. Levy, Chem. Mater. 12 (2000) 2763-2769;
<https://doi.org/10.1021/cm001061z>

[36] S. Baskar, S. Yuvaraj, M. Sundararajan, and C.S. Dash, J. Supercond. Novel Mag. (2020): 1-8; <https://doi.org/10.1007/s10948-020-05665-1>

[37] X. Peng, J. Cheng, J. Yuan, N. Jin, J. Kang, Y. Hou, Q. Zhang, Adv. Appl Ceram, 117(5) (2018) 303-311; <https://doi.org/10.1080/17436753.2017.1410941>

[38] A.T. Dhiwahar, M. Sundararajan, P. Sakthivel, C.S. Dash, and S. Yuvaraj. J. Phy. Chem. Solids 138 (2020): 109257; <https://doi.org/10.1016/j.jpics.2019.109257>

[39] R. Jothiramalingam, T. Radhika, P. R. Aswini, H. Al-Lohedana, M. Chandrasekaran, D. M. Al-Dhayan, J. N. Appaturi, Digest Journal of Nanomaterials and Biostructures, Vol. 17, No. 2, April - June 2022, p. 491 – 497; <https://doi.org/10.15251/DJNB.2022.172.491>

[40] M. Sundararajan, J. Vidhya, R. Revathi, M. Sukumar, V. Ravi, R. Rajkumar, M. Kamalakannan, C. S. Dash, H. Lohedan, R. Jothi Ramalingam, S. Arokiyaraj, J. Ovonic Research, Vol. 17, No. 5, September - October 2021, 479 - 486;
<https://doi.org/10.15251/JOR.2021.175.479>